Letter

Magnetically switchable spin-wave retarder with 90° antiferromagnetic domain wall

Feiyang Ye (叶飞扬) and Jin Lan (兰金)*

Center for Joint Quantum Studies and Department of Physics, School of Science, Tianjin University, 92 Weijin Road, Tianjin 300072, China

(Received 7 July 2021; revised 7 September 2021; accepted 20 October 2021; published 1 November 2021)

Polarization, denoting the precession direction with respect to the background magnetization, is an intrinsic degree of freedom of a spin wave. Using magnetic textures to control the spin-wave polarization is fundamental and indispensable toward reprogrammable polarization-based magnonics. Here, we show that due to the intrinsic cubic anisotropy, a 90° antiferromagnetic domain wall naturally acts as a spin-wave retarder (waveplate). Moreover, for a 90° domain wall pair developed by introducing a second domain in a homogenous antiferromagnetic wire, the sign of the retarding effect can be flipped by simply switching the magnetization direction of the intermediate domain.

DOI: 10.1103/PhysRevB.104.L180401

Introduction. The core issue of current information technology is the enormous power dissipation in signal processing. In conventional electronics, since bits are typically encoded in high/low voltages, heat is unavoidably generated in signal switching due to repeated charging/discharging [1,2]. To ease the dynamical dissipation caused by an imbalanced energy flow, it is natural to encode the binary information in the spin or polarization, as routinely implemented in spintronics [3,4], optics [5,6], acoustics [7], as well as magnonics [8–13] focusing on spin-wave manipulation.

Due to its intrinsic magnetic nature, a spin wave can seamlessly interact with a magnetic texture, and together they provide an integrated scheme for information harnessing in a purely magnetic way [14–17]. With fully unlocked polarization for a spin wave in antiferromagnets [10,18–22], their interplay features are remarkably enriched. The antiferromagnetic skyrmion is shown to induce a polarization-dependent magnon Hall effect [23,24], and a uniaxial 180° antiferromagnetic domain wall with the Dzyaloshinskii-Moriya interaction (DMI) can induce spin-wave polarizing and retarding [9], as well as double refraction [25]. Conversely, the motion of the domain wall in antiferromagnets can be also controlled via simply tuning the spin-wave polarization [26–28].

Despite the flexibility endowed by the polarization from the spin-wave side, the development of purely magnetic logic devices is still much impeded by the lack of enough reprogrammability from the magnetic texture side. Indeed, the logic functions of current magnetic devices are mostly realized by the trivial existence/absence of magnetic textures [29–31]. A promising candidate with intrinsic reprogrammability is the 90° domain wall with multiple variants in materials with cubic magnetic axes, including $CoFe_2O_4$ [32], Fe [33], cubic NiO [34], Heusler alloys [35], Mn_2Au [36], and CuMnAs [37]. The 90° domain wall has been studied both experimentally and theoretically, including spin-wave guiding [14] and refraction [38], and domain wall motion driven by an electric current [39] or spin-orbit field [40,41]. However, efforts in incorporating both 90° domain walls and polarized spin waves to fully unleash the power of magnetic reprogrammability are still lacking.

In this Letter, we investigate the scattering behaviors of a polarized spin wave across a 90° antiferromagnetic domain wall. We show that due to the underlying cubic anisotropy, a 90° antiferromagnetic domain wall shifts the relative phase between two orthogonal linear spin-wave modes. We further propose that a 90° domain wall pair functions as a reprogrammable spin-wave retarder (waveplate), where the sign of the retarding effect can be flipped via switching the central domain direction. Using cubic anisotropic antiferromagnets for spin-wave manipulation extends the current wisdom of designing magnetic devices based on easy-axis or easy-plane magnets [17,42–45].

Basic model. Consider an antiferromagnetic wire with cubic anisotropy lying along the x axis as shown in Fig. 1, where the red (blue) arrows denote the magnetization $\mathbf{m}_{1/2}$ in two sublattices, respectively. We define the normalized staggered order $\mathbf{n} = (\mathbf{m}_1 - \mathbf{m}_2)/|\mathbf{m}_1 - \mathbf{m}_2|$, and the total magnetization $\mathbf{m} = \mathbf{m}_1 + \mathbf{m}_2$. Under the orthogonal constraint $\mathbf{n}\cdot\mathbf{m} = 0$, the dynamics of the staggered order $\mathbf{n}$ is governed by the Landau-Lifshitz-Gilbert (LLG) equation for antiferromagnets [26,27,40,46,47]

$$\mathbf{n}\times\ddot{\mathbf{n}} = \gamma J\mathbf{n}\times(\gamma\mathbf{h} - \alpha\dot{\mathbf{n}}), \tag{1}$$

where $\dot{\mathbf{n}} \equiv \partial_t\mathbf{n}$, $\ddot{\mathbf{n}} \equiv \partial_t^2\mathbf{n}$, γ is the gyromagnetic ratio, α is the Gilbert damping constant, and $\mathbf{h} = -(1/\mu_0 M_s)\delta U/\delta\mathbf{n}$ is the effective magnetic field acting upon $\mathbf{n}$, with μ_0 the vacuum permeability and M_s the saturation magnetization. The magnetic energy U consists of the exchange coupling and cubic anisotropy contributions, $U = U_e + U_c = (\mu_0 M_s/2)\int dx[J\mathbf{m}^2 + A(\partial_x\mathbf{n})^2 + K(n_x^2n_y^2 + n_y^2n_z^2 + n_x^2n_z^2)]$, where J and A are the inter/intra-sublattice exchange constants, and $K > 0$ is the cubic anisotropy constant

*Corresponding author: lanjin@tju.edu.cn

 ©2021 American Physical Society

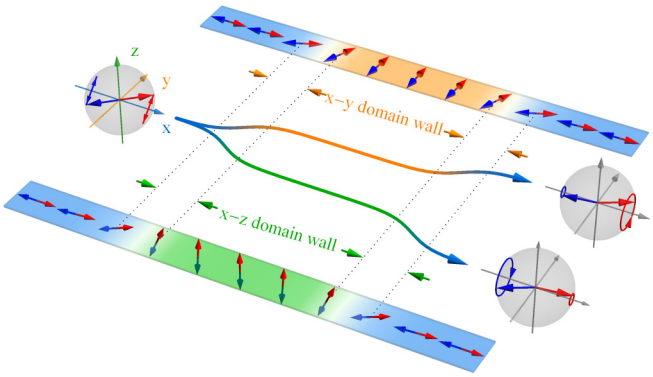

FIG. 1. Schematics of a magnetically switchable spin-wave retarder (waveplate) in cubic anisotropic antiferromagnets. By preparing a y/z domain in the center of a homogeneous x domain, a 90° antiferromagnetic domain wall pair of x-y-x (or x-z-x) type forms. The spin-wave retarding effect of such a structure can be magnetically switched: By changing the intermediate domain to $\hat{\mathbf{y}}/\hat{\mathbf{z}}$ directions, the linear spin wave is transformed to left/right circular spin waves, respectively.

[41,48]. Due to interweaving sublattices, the long-range dipolar interaction is neglected in this antiferromagnetic environment.

The energy contour of cubic anisotropy in a magnetic Bloch sphere is shown in Fig. 2(a), where only one-eighth of the sphere is depicted due to the mirror symmetry with respect to all three Cartesian axes $\hat{\mathbf{x}}_i = \{\hat{\mathbf{x}}, \hat{\mathbf{y}}, \hat{\mathbf{z}}\}$. For convenience, we further denote $i, j, k = \{1, 2, 3\}$ as three different indices obeying the relation $\hat{\mathbf{x}}_i \times \hat{\mathbf{x}}_j = \varepsilon_{ijk}\hat{\mathbf{x}}_k$ with ε_{ijk} the Levi-Civita symbol. As demonstrated, the cubic anisotropic energy U_c minimizes for magnetization $\mathbf{n}$ with one pure Cartesian component $|n_i| = 1$ and $n_j = n_k = 0$, increases when the magnetization has mixed components, and maximizes for the magnetization with equal components $|n_i| = |n_j| = |n_k| = 1/\sqrt{3}$. According to the above features of cubic anisotropy, there are three different magnetic domains in the $\hat{\mathbf{x}}_i$ ($i = 1, 2, 3$) direction as the ground state. When the x_i domain and x_j domain meet, a 90° domain wall arises with its magnetization lying in the x_i-x_j plane, and the out-of-plane magnetization component vanishes with $n_k = 0$.

Under cubic anisotropy, a 180° domain wall in between the $\pm\hat{\mathbf{x}}_i$ domains is not stable, and naturally splits into two separate 90° domain walls, thus it is excluded here [49,50]. For simplicity, we refer to the domains pointing in both $\pm\hat{\mathbf{x}}_i$ directions as the x_i domain, since here their difference in polarization manipulation is minor.

Polarization-dependent spin-wave scattering. When a spin wave is excited within a uniform domain, its two linear polarization modes are degenerate since the cubic anisotropy is invariant under the interchange of any two axes, as shown in Fig. 2(a). As the spin wave propagates upon the domain wall, these two linear polarizations become in-plane and out-of-plane modes in reference to the domain wall plane, as illustrated in Fig. 2(b). For in-plane modes, magnetization oscillations upon the domain wall are still with two magnetization components, thus the spin-wave dynamics is almost unaffected by the cubic anisotropy, while the out-of-plane modes involve the third magnetization component, and thus are subject to an additional suppression of the cubic anisotropy. Due to the distinct behaviors of in-plane and out-of-plane modes under cubic anisotropy, polarization-dependent spin-wave scattering thus arises in a 90° domain wall.

To proceed with the investigations on the spin-wave scattering, we denote the 90° domain wall as $\mathbf{n}_0$, and the spin wave as $\delta\mathbf{n} = n_\parallel\hat{\mathbf{e}}_\parallel + n_\perp\hat{\mathbf{e}}_\perp$, where $\hat{\mathbf{e}}_\parallel$ and $\hat{\mathbf{e}}_\perp$ are the in-plane and out-of-plane directions with respect to the domain wall plane subtended by $\mathbf{n}_0$. For the x-y domain wall, its magnetic profile is $\mathbf{n}_0 = (\sqrt{[1-\tanh(x/W)]/2}, \sqrt{[1+\tanh(x/W)]/2}, 0)$, with $W = \sqrt{A/K}$ the characteristic width, and the x-z (y-z) domain walls take a similar form [39]. With the above domain wall profile, the spin-wave dynamics is then recast from LLG

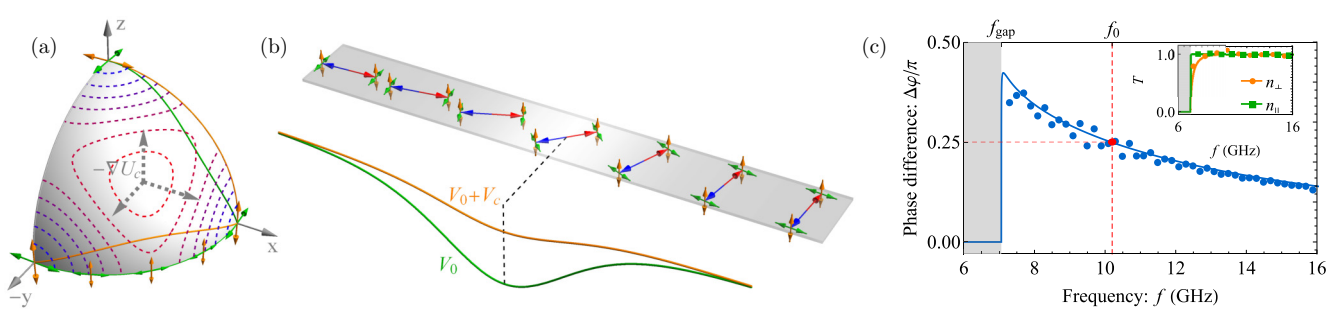

FIG. 2. The retarding effect of a 90° domain wall. (a) Contour plots of the cubic anisotropy energy in a Bloch sphere. The green/orange arrows denote the two polarization directions of spin waves, and the green/orange solid lines plot the corresponding total magnetization projected in the Bloch sphere. (b) Schematics of polarized spin waves in a 90° domain wall. The red/blue arrows denote the domain wall magnetizations in two sublattices, and the green/orange arrows depict two linearly polarized spin waves. The green/orange lines plot the effective potentials experienced by the in-plane and out-of-plane spin-wave modes. (c) The interpolarization phase difference $\Delta\varphi$ as a function of spin-wave frequency. The solid line plots the full-scattering calculations [51], and the dots are extracted from micromagnetic simulations. The red dot denotes the working frequency $f_0 = 10.2$ GHz for the 90° domain wall acting as a one-eighth waveplate. Inset: The transmission probability T for $n_\parallel$ (green) and $n_\perp$ (orange), respectively. The calculations are based on a synthetic antiferromagnet [33,52] with the following magnetic parameters: the inter/intra-sublattice exchange coupling constants $J = 1 \times 10^6$ A/m and $A = 3.28 \times 10^{-11}$ A m, the cubic anisotropy constant $K = 3.88 \times 10^4$ A/m, and the gyromagnetic ratio $\gamma = 2.21 \times 10^5$ Hz/(A/m).

equation (1) to Klein-Gordon-like equations,

$$-\ddot{n}_{\parallel} = \gamma^2 J\left[-A\partial_x^2 + V_0(x)\right]n_{\parallel}, \tag{2a}$$

$$-\ddot{n}_{\perp} = \gamma^2 J\left[-A\partial_x^2 + V_0(x) + V_c(x)\right]n_{\perp}, \tag{2b}$$

where the potential $V_0 = K[1 - 2\,\mathrm{sech}^2(x/W)]$ is caused by the inhomogeneous domain wall profile, and $V_c = (5/4)K\,\mathrm{sech}^2(x/W)$ solely emerging for the out-of-plane mode is induced by the cubic anisotropy. The potential V_0 is the celebrated Pöschl-Teller type potential sharing the same profile as the 180° domain wall case [26,27,53,54], which always passes the spin wave perfectly.

From Eq. (2), in homogeneous domains far away from the domain wall ($|x| \gg W$), the in-plane and out-of-plane modes are degenerate with the dispersion relation $\omega = \gamma\sqrt{J(Ak^2 + K)}$, with ω the spin-wave frequency and k the wave vector. Inside the domain wall, the degeneracy of the two modes is lifted by the potential V_c, leading to a phase difference accumulated between two modes across the domain wall. Figure 2(c) plots the interpolarization phase difference $\Delta\varphi \equiv \varphi_{\perp} - \varphi_{\parallel}$ obtained from full-scattering calculations [51,55] and extracted from micromagnetic simulations, which overlap well with each other. The positive phase difference $\Delta\varphi > 0$, together with an almost perfect transmission of both modes (except for some reflections in the low-frequency range) as demonstrated in Fig. 2(c), corroborate the retarding effect of the 90° domain wall.

For the x_i-x_j domain wall, the out-of-plane direction is always $\hat{\mathbf{e}}_{\perp} = \hat{\mathbf{x}}_k$, while the in-plane direction gradually changes $\hat{\mathbf{e}}_{\parallel} = \hat{\mathbf{x}}_j \to \hat{\mathbf{x}}_i$, indicating a rotation of the polarization basis. In addition, for x_i-x_j and x_i-x_k domain walls starting from the same x_i domain, the roles of linear-x_j (linear-x_k) modes as the in-plane (out-of-plane) mode are exchanged, as illustrated in Fig. 2(a) [51]. Moreover, when the linear-x_j (linear-x_k) mode penetrates through three cyclically connected x_i-x_j-x_k-x_i domain walls, it is transformed into the orthogonal linear-x_k (linear-x_j) mode rather than restoring its original polarization direction. These unique polarization basis variation features in cubic anisotropic systems highlight the non-Abelian behaviors of SU(2) spin rotation [56].

Spin-wave retarder. The rotation of the polarization basis together with the phase difference $\Delta\varphi$ indicate that a 90° domain wall acts as a rotated retarder [57] for the spin wave. For pure retarding functionality, a pair of 90° domain walls is necessary, where the basis rotation is canceled, while the phase difference is doubled. Such a domain wall pair can be straightforwardly prepared by placing a second domain in a homogeneous magnetic wire, as illustrated in Fig. 1. In between two x_i domains, the intermediate domain may either be an x_j domain or x_k domain to form such a domain wall pair. And for these two configurations, the in-plane and out-of-plane directions are exchanged, leading to the opposite sign of the phase difference between the linear-x_j and linear-x_k components, i.e., $\Delta\phi \equiv \varphi_k - \varphi_j = \pm 2\Delta\varphi$ (see details in Fig. S1 [51]).

The retarding effect of the domain wall pair is verified by micromagnetic simulations, as plotted in Fig. 3. A 45°-linear spin wave with a working frequency $f_0 = 10.2$ GHz is injected from the left side of an x-y-x (or x-z-x) domain wall pair. The phase difference $\Delta\phi$ levels off inside each domain, but increases/decreases by $\pi/4$ as the spin wave passes through each x-y (or x-z) domain wall in Fig. 3(a). After the spin wave reaches the x domain on the right side, it acquires a phase difference of $\pm\pi/2$ as expected, indicating that the 45°-linear spin wave becomes left/right circularly polarized, respectively. Typical snapshots of a spin wave propagating in the domain wall pair are further depicted in Fig. 3(b). For convenience, we denote $n'_{y/z}$ as extensions of the spin-wave components $n_{y/z}$ in the x domain to the whole domain wall pair region. While overlapping on the left side, the n'_y component lags/advances the n'_z component as the spin wave penetrates through the x-y-x (or x-z-x) domain wall pair, highlighting their opposite retarding effects.

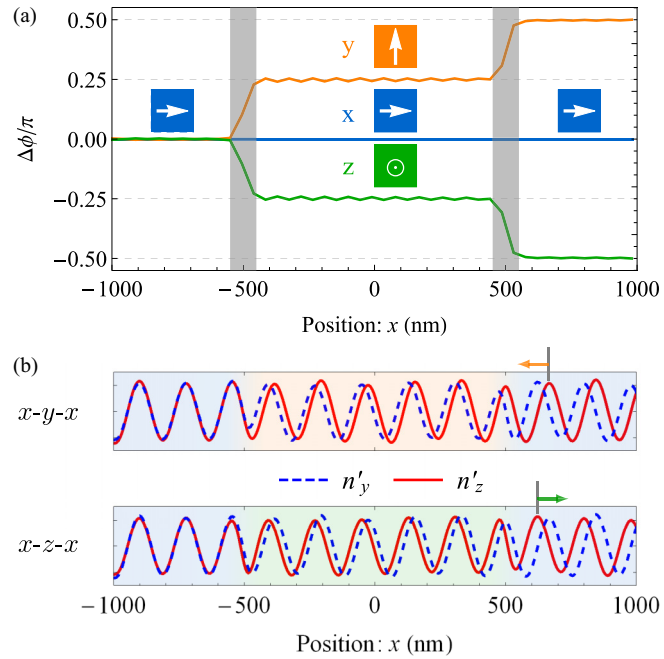

FIG. 3. Micromagnetic simulations of the spin-wave retarder based on a domain wall pair. (a) The spatial evolution of the interpolarization phase difference $\Delta\phi$ extracted from micromagnetic simulations. The orange/green lines are for the x-$y(z)$-x domain wall pair, and the blue line is for the homogenous x domain for reference. (b) The spatial profile of the spin-wave components in the x-y-x (upper panel) and x-z-x (lower panel) domain wall pair. The blue/red lines plot the n'_y and n'_z components, which refers to $n_{y/z}$ in the x domain and their extensions within the domain wall pair. In (a) and (b), two domain walls are located at $x = \pm 500$ nm, the spin-wave frequency is $f = 10.2$ GHz, the magnetic parameters follow Fig. 2, and the damping constant is artificially set to $\alpha = 0$ for better demonstration of the retarding effect.

Magnetic reprogrammability. The antiferromagnetic domain can be switched to different directions by exerting an effective Néel-order magnetic field induced by current pulses [34,36,37,58,59]. By rewriting the central domain using such a staggered field, the retarding effect of the domain wall pair is then reprogrammed, as shown in Fig. 4. When a Néel-order magnetic field $\mathbf{H}^N = H_y^N\hat{\mathbf{y}}$ of duration 1 ns is applied, the central domain quickly switches from the $\hat{\mathbf{x}}$ direction to the designated $\mathbf{n}_0 = \hat{\mathbf{y}}$ direction after a stabilization time of 2 ns, and the spin-wave phase difference $\Delta\phi$ quickly changes from

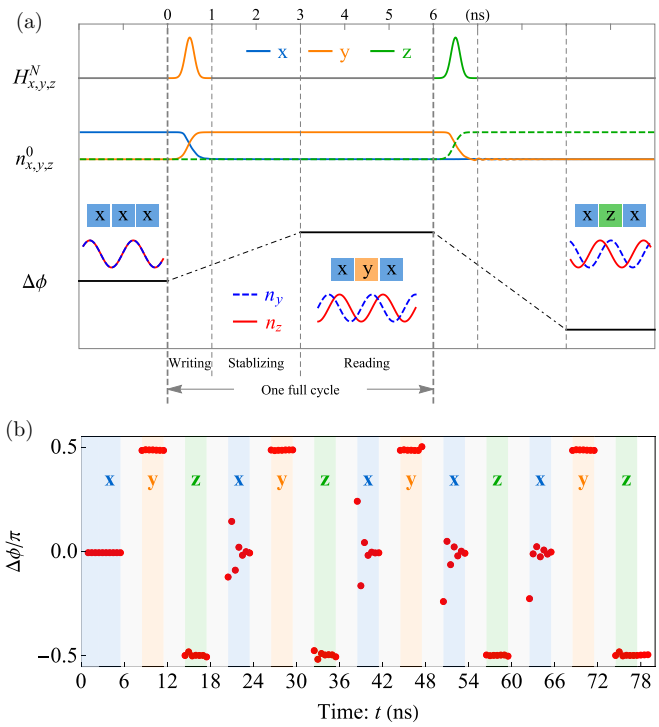

FIG. 4. Reprogrammable spin-wave retarder by switching the magnetization of the central domain. (a) Timing diagram of magnetic signals in one programming cycle of 6 ns. A Néel-order magnetic field $\mathbf{H}^N$ is applied at [0, 1] ns for central domain writing, and the magnetic structure $\mathbf{n}_0$ waits for stabilization at [1, 3] ns, while the interpolarization phase difference $\Delta\phi$ is read at [3, 6] ns. The insets schematically show the state of the domain wall pair, and the spatial profile of two spin-wave components at the right x domain. (b) Time evolution of the phase difference $\Delta\phi$ in 12 programming cycles. The red dots are the phase difference extracted from the simulations, and the background blue/orange/green colors are for the stabilized $x/y/z$ domain, respectively. In (a) and (b), the magnetic wire lies at $[-1000, 1000]$ nm, the domain walls are prepared at ± 350 nm, the 45°-linear spin wave with frequency $f = 10.2$ GHz is continuously excited at $x = -500$ nm, and the output spin wave is read at $x = 600$ nm. The Gilbert damping constant inside the wire is $\alpha = 1.4 \times 10^{-2}$, and is increased to $\alpha = 0.1$ near the boundaries ($|x| > 900$ nm) to absorb redundant spin waves.

0 to 0.5π in Fig. 4(a). The signals in the last 3 ns of the 6 ns full cycle become stable and clean, thus the retarder is ready for the next programming cycle.

In Fig. 4(b), a train of 12 external field pulses is applied to switch the central domain arbitrarily between three orthogonal directions [51]. For all 12 cycles, the output phase difference $\Delta\phi$ steadily switches to 0 or $\pm\pi/2$, when the central domain is stabilized in the $\hat{\mathbf{x}}/\hat{\mathbf{y}}/\hat{\mathbf{z}}$ directions. The switching to the central x domain corresponds to the elimination of the domain wall pair, thus abundant spin waves are released, leading to a slightly lower signal quality. Despite the fluctuations, the phase difference $\Delta\phi$ still clearly falls into three well-separated ranges, highlighting the robustness of the reprogrammable retarder.

Discussion. The retarding effect also arises in the 180° domain wall with easy-axis anisotropy in Ref. [9], but the underlying mechanisms are distinct: The degeneracy of polarizations is lifted by the intrinsic cubic anisotropy in this work, but relies on the external DMI in Ref. [9]. In addition, the cubic anisotropy preserves high symmetry, while the DMI conversely requires one to break the inversion symmetry. The involvement of only the exchange coupling and cubic anisotropy also implies that the retarding effect in this work is universally applicable to all cubic anisotropic antiferromagnets.

To switch the domain wall pair between two configurations (e.g., x-y-x and x-z-x configurations), one simply needs to change the magnetic state of the central domain. These two configurations are symmetric with each other, sharing a similar structure and exactly the same energy, but introducing the opposite retarding effect. In this sense, the reprogrammability demonstrated here is truly symmetric, and distinguishes from previous proposals simply based on the presence/absence states. To guarantee the symmetry of the reprogrammability, triplet degeneracy is required, with one state as the reference and the other two for switching, e.g., the triple equivalent domains hosted by the cubic anisotropy. The spirit of symmetric reprogrammability thus coincides with the polarization (spin)-based manipulations via exploring the additional degree of freedom, rather than breaking symmetry in the existing degrees of freedom.

Toward experiments. The polarized spin wave can be excited by applying an oscillating magnetic field via an antenna, and then can be detected via the antiferromagnetic spin pumping by attaching an adjacent Pt layer [18,60], which converts the left/right circular polarizations to positive/negative electrical signals. In addition, the application of a global Néel-order magnetic field should remove remanent multidomains in the wire.

Conclusion. In conclusion, we demonstrate that a 90° antiferromagnetic domain wall pair naturally functions as a reprogrammable spin-wave retarder. By switching the magnetic direction of the central domain, the linear spin wave can be converted to either a left- or right-circular mode. Due to the rich functionality and embedded reprogrammability, the cubic anisotropic antiferromagnet manifests as another platform for magnetic information processing.

Acknowledgments. J.L. is grateful to Jiang Xiao for insightful discussions. This work is supported by the National Natural Science Foundation of China (No. 11904260), the Natural Science Foundation of Tianjin (No. 20JCQNJC02020), and the Startup Fund of Tianjin University.

[1] M. Lundstrom, Moore's law forever? Science **299**, 210 (2003).

[2] I. L. Markov, Limits on fundamental limits to computation, Nature (London) **512**, 147 (2014).

[3] S. Wolf, D. Awschalom, R. Buhrman, J. Daughton, S. von Molnár, M. Roukes, A. Chtchelkanova, and D. Treger, Spintronics: a spin-based electronics vision for the future, Science **294**, 1488 (2001).

[4] I. Žutić, J. Fabian, and S. Das Sarma, Spintronics: Fundamentals and applications, Rev. Mod. Phys. **76**, 323 (2004).
[5] C. H. Bennett and D. P. DiVincenzo, Quantum information and computation, Nature (London) **404**, 247 (2000).
[6] J. P. Balthasar Mueller, N. A. Rubin, R. C. Devlin, B. Groever, and F. Capasso, Metasurface Polarization Optics: Independent Phase Control of Arbitrary Orthogonal States of Polarization, Phys. Rev. Lett. **118**, 113901 (2017).
[7] M. C. Kuzyk and H. Wang, Scaling Phononic Quantum Networks of Solid-State Spins with Closed Mechanical Subsystems, Phys. Rev. X **8**, 041027 (2018).
[8] R. Cheng, M. W. Daniels, J.-G. Zhu, and D. Xiao, Antiferromagnetic spin wave field-effect transistor, Sci. Rep. **6**, 24223 (2016).
[9] J. Lan, W. Yu, and J. Xiao, Antiferromagnetic domain wall as spin wave polarizer and retarder, Nat. Commun. **8**, 178 (2017).
[10] J. Li, C. B. Wilson, R. Cheng, M. Lohmann, M. Kavand, W. Yuan, M. Aldosary, N. Agladze, P. Wei, M. S. Sherwin, and J. Shi, Spin current from sub-terahertz-generated antiferromagnetic magnons, Nature (London) **578**, 70 (2020).
[11] S. M. Rezende, R. L. Rodríguez-Suárez, and A. Azevedo, Diffusive magnonic spin transport in antiferromagnetic insulators, Phys. Rev. B **93**, 054412 (2016).
[12] S. A. Bender, H. Skarsvåg, A. Brataas, and R. A. Duine, Enhanced Spin Conductance of a Thin-Film Insulating Antiferromagnet, Phys. Rev. Lett. **119**, 056804 (2017).
[13] R. Lebrun, A. Ross, S. Bender, A. Qaiumzadeh, L. Baldrati, J. Cramer, A. Brataas, R. Duine, and M. Kläui, Tunable long-distance spin transport in a crystalline antiferromagnetic iron oxide, Nature (London) **561**, 222 (2018).
[14] J. Lan, W. Yu, R. Wu, and J. Xiao, Spin-Wave Diode, Phys. Rev. X **5**, 041049 (2015).
[15] J. Han, P. Zhang, J. T. Hou, S. A. Siddiqui, and L. Liu, Mutual control of coherent spin waves and magnetic domain walls in a magnonic device, Science **366**, 1121 (2019).
[16] W. Yu, J. Lan, and J. Xiao, Magnetic Logic Gate Based on Polarized Spin Waves, Phys. Rev. Applied **13**, 024055 (2020).
[17] H. Yu, J. Xiao, and H. Schultheiss, Magnetic texture based magnonics, Phys. Rep. **905**, 1 (2021).
[18] R. Cheng, J. Xiao, Q. Niu, and A. Brataas, Spin Pumping and Spin-Transfer Torques in Antiferromagnets, Phys. Rev. Lett. **113**, 057601 (2014).
[19] S. M. Wu, W. Zhang, A. KC, P. Borisov, J. E. Pearson, J. S. Jiang, D. Lederman, A. Hoffmann, and A. Bhattacharya, Antiferromagnetic Spin Seebeck Effect, Phys. Rev. Lett. **116**, 097204 (2016).
[20] I. Proskurin, R. L. Stamps, A. S. Ovchinnikov, and J.-i. Kishine, Spin-Wave Chirality and Its Manifestations in Antiferromagnets, Phys. Rev. Lett. **119**, 177202 (2017).
[21] X.-X. Zhang, L. Li, D. Weber, J. Goldberger, K. F. Mak, and J. Shan, Gate-tunable spin waves in antiferromagnetic atomic bilayers, Nat. Mater. **19**, 838 (2020).
[22] M. Ishibashi, Y. Shiota, T. Li, S. Funada, T. Moriyama, and T. Ono, Switchable giant nonreciprocal frequency shift of propagating spin waves in synthetic antiferromagnets, Sci. Adv. **6**, 17 (2020).
[23] M. W. Daniels, W. Yu, R. Cheng, J. Xiao, and D. Xiao, Topological spin Hall effects and tunable skyrmion Hall effects in uniaxial antiferromagnetic insulators, Phys. Rev. B **99**, 224433 (2019).
[24] S. K. Kim, K. Nakata, D. Loss, and Y. Tserkovnyak, Tunable Magnonic Thermal Hall Effect in Skyrmion Crystal Phases of Ferrimagnets, Phys. Rev. Lett. **122**, 057204 (2019).
[25] J. Lan, W. Yu, and J. Xiao, Geometric magnonics with chiral magnetic domain walls, Phys. Rev. B **103**, 214407 (2021).
[26] E. G. Tveten, A. Qaiumzadeh, and A. Brataas, Antiferromagnetic Domain Wall Motion Induced by Spin Waves, Phys. Rev. Lett. **112**, 147204 (2014).
[27] W. Yu, J. Lan, and J. Xiao, Polarization-selective spin wave driven domain-wall motion in antiferromagnets, Phys. Rev. B **98**, 144422 (2018).
[28] A. Qaiumzadeh, L. A. Kristiansen, and A. Brataas, Controlling chiral domain walls in antiferromagnets using spin-wave helicity, Phys. Rev. B **97**, 020402(R) (2018).
[29] R. Hertel, W. Wulfhekel, and J. Kirschner, Domain-Wall Induced Phase Shifts in Spin Waves, Phys. Rev. Lett. **93**, 257202 (2004).
[30] X. Zhang, M. Ezawa, and Y. Zhou, Magnetic skyrmion logic gates: conversion, duplication and merging of skyrmions, Sci. Rep. **5**, 9400 (2015).
[31] M. Chauwin, X. Hu, F. Garcia-Sanchez, N. Betrabet, A. Paler, C. Moutafis, and J. S. Friedman, Skyrmion Logic System for Large-Scale Reversible Computation, Phys. Rev. Appl. **12**, 064053 (2019).
[32] R. M. Bozorth, E. F. Tilden, and A. J. Williams, Anisotropy and magnetostriction of some ferrites, Phys. Rev. **99**, 1788 (1955).
[33] J. J. Krebs, P. Lubitz, A. Chaiken, and G. A. Prinz, Magnetic Resonance Determination of the Antiferromagnetic Coupling of Fe Layers Through Cr, Phys. Rev. Lett. **63**, 1645 (1989).
[34] L. Baldrati, O. Gomonay, A. Ross, M. Filianina, R. Lebrun, R. Ramos, C. Leveille, F. Fuhrmann, T. R. Forrest, F. Maccherozzi, S. Valencia, F. Kronast, E. Saitoh, J. Sinova, and M. Kläui, Mechanism of Néel Order Switching in Antiferromagnetic Thin Films Revealed by Magnetotransport and Direct Imaging, Phys. Rev. Lett. **123**, 177201 (2019).
[35] K. O'Grady, J. Sinclair, K. Elphick, R. Carpenter, G. Vallejo-Fernandez, M. I. J. Probert, and A. Hirohata, Anisotropy in antiferromagnets, J. Appl. Phys. **128**, 040901 (2020).
[36] J. Železný, H. Gao, K. Výborný, J. Zemen, J. Mašek, A. Manchon, J. Wunderlich, J. Sinova, and T. Jungwirth, Relativistic Néel-Order Fields Induced by Electrical Current in Antiferromagnets, Phys. Rev. Lett. **113**, 157201 (2014).
[37] P. Wadley, B. Howells, J. Železný, C. Andrews, V. Hills, R. P. Campion, V. Novák, K. Olejník, F. Maccherozzi, S. S. Dhesi, S. Y. Martin, T. Wagner, J. Wunderlich, F. Freimuth, Y. Mokrousov, J. Kuneš, J. S. Chauhan, M. J. Grzybowski, A. W. Rushforth, K. W. Edmonds, B. L. Gallagher, and T. Jungwirth, Electrical switching of an antiferromagnet, Science **351**, 587 (2016).
[38] T. Hioki, R. Tsuboi, T. H. Johansen, Y. Hashimoto, and E. Saitoh, Snell's law for spin waves at a 90° magnetic domain wall, Appl. Phys. Lett. **116**, 112402 (2020).
[39] E. G. Tveten, A. Qaiumzadeh, O. A. Tretiakov, and A. Brataas, Staggered Dynamics in Antiferromagnets by Collective Coordinates, Phys. Rev. Lett. **110**, 127208 (2013).
[40] O. Gomonay, T. Jungwirth, and J. Sinova, High Antiferromagnetic Domain Wall Velocity Induced by Néel Spin-Orbit Torques, Phys. Rev. Lett. **117**, 017202 (2016).

[41] H. Yang, H. Y. Yuan, M. Yan, H. W. Zhang, and P. Yan, Atomic antiferromagnetic domain wall propagation beyond the relativistic limit, Phys. Rev. B **100**, 024407 (2019).

[42] S. S. P. Parkin, M. Hayashi, and L. Thomas, Magnetic domain-wall racetrack memory, Science **320**, 190 (2008).

[43] S. S. P. Parkin and S.-H. Yang, Memory on the racetrack, Nat. Nanotechnol. **10**, 195 (2015).

[44] D. Hill, S. K. Kim, and Y. Tserkovnyak, Spin-Torque-Biased Magnetic Strip: Nonequilibrium Phase Diagram and Relation to Long Josephson Junctions, Phys. Rev. Lett. **121**, 037202 (2018).

[45] J. Han, P. Zhang, Z. Bi, Y. Fan, T. S. Safi, J. Xiang, J. Finley, L. Fu, R. Cheng, and L. Liu, Birefringence-like spin transport via linearly polarized antiferromagnetic magnons, Nat. Nanotechnol. **15**, 563 (2020).

[46] T. Shiino, S.-H. Oh, P. M. Haney, S.-W. Lee, G. Go, B.-G. Park, and K.-J. Lee, Antiferromagnetic Domain Wall Motion Driven by Spin-Orbit Torques, Phys. Rev. Lett. **117**, 087203 (2016).

[47] E. G. Tveten, T. Müller, J. Linder, and A. Brataas, Intrinsic magnetization of antiferromagnetic textures, Phys. Rev. B **93**, 104408 (2016).

[48] D. Stancil and A. Prabhakar, *Spin Waves: Theory and Applications* (Springer, New York, 2009).

[49] Q.-f. Zhan, S. Vandezande, K. Temst, and C. Van Haesendonck, Magnetic anisotropy and reversal in epitaxial Fe/MgO(001) films, Phys. Rev. B **80**, 094416 (2009).

[50] S. Mallik, N. Chowdhury, and S. Bedanta, Interplay of uniaxial and cubic anisotropy in epitaxial Fe thin films on MgO (001) substrate, AIP Adv. **4**, 097118 (2014).

[51] See Supplemental Material at http://link.aps.org/supplemental/10.1103/PhysRevB.104.L180401 for more details of micromagnetic simulations, full-scattering calculations, spin-wave polarizations in the 90° domain wall pair, working principles, and a movie of the switchable spin-wave retarder, which includes Refs. [9,27,47,54,55].

[52] R. A. Duine, K.-J. Lee, S. S. P. Parkin, and M. D. Stiles, Synthetic antiferromagnetic spintronics, Nat. Phys. **14**, 217 (2018).

[53] P. Yan, X. S. Wang, and X. R. Wang, All-Magnonic Spin-Transfer Torque and Domain Wall Propagation, Phys. Rev. Lett. **107**, 177207 (2011).

[54] S. K. Kim, Y. Tserkovnyak, and O. Tchernyshyov, Propulsion of a domain wall in an antiferromagnet by magnons, Phys. Rev. B **90**, 104406 (2014).

[55] P. A. Khomyakov, G. Brocks, V. Karpan, M. Zwierzycki, and P. J. Kelly, Conductance calculations for quantum wires and interfaces: Mode matching and Green's functions, Phys. Rev. B **72**, 035450 (2005).

[56] D. Xiao, M.-C. Chang, and Q. Niu, Berry phase effects on electronic properties, Rev. Mod. Phys. **82**, 1959 (2010).

[57] D. H. Goldstein, *Polarized Light* (CRC Press, Boca Raton, FL, 2003).

[58] Y. Cheng, S. Yu, M. Zhu, J. Hwang, and F. Yang, Electrical Switching of Tristate Antiferromagnetic Néel Order in α-Fe_2O_3 Epitaxial Films, Phys. Rev. Lett. **124**, 027202 (2020).

[59] S. Y. Bodnar, L. Šmejkal, I. Turek, T. Jungwirth, O. Gomonay, J. Sinova, A. Sapozhnik, H.-J. Elmers, M. Kläui, and M. Jourdan, Writing and reading antiferromagnetic Mn_2Au by Néel spin-orbit torques and large anisotropic magnetoresistance, Nat. Commun. **9**, 348 (2018).

[60] P. Vaidya, S. A. Morley, J. van Tol, Y. Liu, R. Cheng, A. Brataas, D. Lederman, and E. del Barco, Subterahertz spin pumping from an insulating antiferromagnet, Science **368**, 160 (2020).